Anticorrosion Coatings with Self-Healing Effect Based on Nanocontainers Impregnated with Corrosion Inhibitor

Mikhail L. Zheludkevich,*,† Dmitry G. Shchukin,‡ Kiryl A. Yasakau,† Helmut Möhwald,‡ and Mario G. S. Ferreira†

Department of Ceramics and Glass Engineering, CICECO, University of Aveiro, 3810-193 Aveiro, Portugal, and Max Planck Institute of Colloids and Interfaces, D14424 Potsdam, Germany

Received August 31, 2006. Revised Manuscript Received November 22, 2006

The development of active corrosion protection systems for metallic substrates is an issue of prime importance for many industrial applications. The present work shows a new contribution to the development of a new protective system with self-healing ability composed of hybrid sol−gel films doped with nanocontainers that release entrapped corrosion inhibitor in response to pH changes caused by corrosion process. A silica−zirconia based hybrid film was used in this work as an anticorrosion coating deposited on 2024 aluminum alloy. Silica nanoparticles covered layer-by-layer with polyelectrolyte layers and layers of inhibitor (benzotriazole) were randomly introduced into the hybrid films. The hybrid film with the nanocontainers reveals enhanced long-term corrosion protection in comparison with the undoped hybrid film. The scanning vibrating electrode technique also shows an effective self-healing ability of the defects. This effect is obtained due to regulated release of the corrosion inhibitor triggered by the corrosion processes started in the cavities. The approach described herein can be used in many applications where active corrosion protection of materials is required.

1. Introduction

Corrosion degradation of materials and structures is one of the important issues that leads to depreciation of investment goods. Two main approaches, an active and a passive one, are currently used for corrosion protection. The passive corrosion protection is achieved by deposition of the barrier layer preventing contact of the material with the corrosive environment.[1] The active corrosion protection aims at a decrease of the corrosion rate when the main barrier is damaged and corrosive species come in contact with the substrate.[2−4] One of the ways to provide an active protection of metals is the introduction of corrosion inhibitors in the system. However, only the combination of both approaches can give reliable long-term corrosion protection of metallic structures which are in contact with electrolytes or a humid environment.[2,3] The corrosion inhibitors can be introduced in the different components of the coating system: pretreatment, primer, and top coat. Inhibiting agents are effective only if their solubility in the corrosive environment is in the right range. Very low solubility of inhibitor leads to lack of active agent at the metal interface and consequently to weak inhibition. If the solubility is too high the substrate will be protected, but for only a relatively short time since the inhibitor will be rapidly leached out from the coating. Another drawback, which can appear because of high solubility, is the osmotic pressure that leads to blistering and delamination of protective coatings. The osmotic pressure can stimulate water to be transported through the coating, which acts as a semipermeable membrane, causing the destruction of the barrier layer (especially for coatings containing molybdates, chromates, and borates). This problem becomes more acute due to the upcoming restriction of the use of chromates, which are known as the most effective inhibitors but are strongly carcinogenic. The development of a new approach to introduce environmentally friendly corrosion inhibitors, which can provide prolonged and even "smart" release of the inhibiting species on demand, becomes an important issue for many industries where an adequate corrosion protection is needed.[2]

Several attempts were made to introduce different species in polymer coatings for controlled release of inhibitor. Buchheit et al.[5] used Al−Zn-decavanadate hydrotalcite as anticorrosion pigment, adding it to epoxy-based organic coating. The Zn^{2+} and vanadate ions can be released from the hydrotalcite seeds when chloride ions reach the coating. In this case, decavanadate ions replaced by chloride decelerate the anodic processes and diminish the corrosion activity.[5] In other work the chemically synthesized hydrocalmite was used as an anion exchanger to adsorb corrosive chloride ions releasing nitrites, which can stop corrosion.[6] The organic triazole inhibitor was encapsulated using plasma polymerization to produce plasma polymerized perfluorohexane and polypyrrole layers.[7] Plasma-treated triazole seeds were used

* Corresponding author. Tel.: +351 234 370 255. Fax: +351 234 378 146. E-mail address: mzheludkevich@cv.ua.pt.
† University of Aveiro.
‡ Max Planck Institute of Colloids and Interfaces.

(1) Brooman, E. W. *Metal Finishing* **2002**, *100* (5), 48.
(2) Brooman, E. W. *Metal Finishing* **2002**, *100* (1), 42.
(3) Brooman, E. W. *Metal Finishing* **2002**, *100* (6), 104.
(4) Roux, S.; Audebert, P.; Pagetti, J.; Roche, M. *J. Mater. Chem.* **2001**, *11*, 3360.
(5) Buchheit, R. G.; Guan, H.; Mahajanam, S.; Wong, F. *Prog. Org. Coat.* **2003**, *47*, 174.
(6) Tatematsu, H.; Sasaki, T. *Cem. Concr. Compos.* **2003**, *25*, 123.
(7) Yang, H.; van Ooij, W. J. *Plasmas Polym.* **2003**, *8*, 297.

10.1021/cm062066k CCC: $37.00 © 2007 American Chemical Society
Published on Web 01/11/2007

as a pigment in a water-based epoxy coating slowly releasing the inhibitor and providing a long-term corrosion protection.

Another promising approach, which allows doping of the protection system without any degradation of the coating integrity, is loading the primer or the pretreatment layer with corrosion inhibitors. The hybrid silane derived thin layers was investigated as prospective pretreatments for many metallic substrates.[8−15] However, interaction of the inhibitors with the sol−gel layer very often leads to significant shortcomings in the stability of the layer and activity of the inhibitor. For example, sol−gel films with $NaVO_3$ and Na_2MoO_4 did not provide adequate corrosion protection due to decrease of the sol−gel network stability.[11] Cerium-based additives work better below a certain critical concentration (0.2−0.6 wt %). Above this concentration the formation of defects occurs in the sol−gel film.[11,13] van Ooij et al. introduced triazole-based organic inhibitors into a hybrid sol−gel matrix.[16,17] Self-healing ability was not revealed in this case probably because of the deactivation of the inhibitor molecules by their interaction with the sol−gel matrix. The rate of release is strongly dependent on the isoelectric points and ζ-potential of the sol−gel matrix and inhibitor.[18] Hence, in many cases the release of the organic inhibitor from the sol−gel film is impossible or very slow.

Low efficiency of the coatings containing inhibitor in their internal structure calls for the development of new approaches that isolate the inhibitor from the coating materials, confining them in nano- and microreservoirs. Their shell can prevent direct interaction of the inhibitor with the layer matrix avoiding the negative effect of inhibiting species on the stability of the anticorrosion coating. Oxide nanoparticles containing cerium ions,[19,20] hollow polypropylene fibers,[21] and β-cyclodextrin-inhibitor complexes[10] were explored as isolated, inhibitor-impregnated reservoirs to be incorporated inside the protective coatings providing prolonged release of the inhibitor and self-healing ability.

Nanocontainers with regulated storage/release of the inhibitor can be fabricated with nanometer-scale precision employing the layer-by-layer (LbL) deposition approach.[22] With this step-by-step deposition of oppositely charged substances (e.g., polyelectrolytes, nanoparticles, biomaterials) from their aqueous and nonaqueous solutions on the surface of a template material LbL films were assembled and investigated as perspective materials in photonics[23] and electrocatalysis[24,25] and as membranes for gas separation[26−29] and spatially confined chemical nanoreactors.[30,31]

LbL films containing one or several polyelectrolyte monolayers assembled on the surface of a sacrificial template (e.g., polyelectrolyte capsules) possess controlled permeability properties. Polyelectrolyte multilayers are permeable toward ions and small organic molecules while large organic molecules (polymers, enzymes) and nanoparticles can be entrapped inside. The permeability of the polyelectrolyte multilayers depends on the nature of the polyelectrolytes. Other constituents of the LbL film can be adjusted by changing the pH (for weak polyelectrolytes), ionic strength (for strong polyelectrolytes), or temperature (in the presence of thermo-responsive polymers) or by applying magnetic or electromagnetic fields (in the presence of magnetic or metal nanoparticles).[32−35] Polyelectrolyte assemblies have not yet been employed as containers for corrosion inhibitors in protection coatings, although storage of corrosion inhibitors in the polyelectrolyte multilayers has two advantages: isolate the inhibitor avoiding its negative effect on the integrity of the coating and provide intelligent release of the corrosion inhibitor by regulation of the permeability of polyelectrolyte assemblies changing local pH, humidity, and irradiation conditions. The change of pH is a more preferable trigger to initiate the release of inhibitor since, as well-known, corrosion activity leads to local changes of pH near cathodic and anodic defects.[36] Thus, a "smart" coating containing polyelectrolyte containers can detect corrosion and start the self-healing process in a corrosion defect.

However, polyelectrolyte containers in anticorrosion coatings have two significant restrictions: they have to be compatible with the material of the protective film to prevent film distortion and have to be nanoscale in size for uniform and closely packed distribution inside the protective coating.

(8) Zheludkevich, M. L.; Salvado, I. M.; Ferreira, M. G. S. *J. Mater. Chem.* **2005**, *15*, 5099.
(9) Kasten, L. S.; Grant, J. T.; Grebasch, N.; Voevodin, N.; Arnold, F. E.; Donley, M. S. *Surf. Coat. Technol.* **2001**, *140*, 11.
(10) Khramov, A. N.; Voevodin, N. N.; Balbyshev, V. N.; Donley, M. S. *Thin Solid Films* **2004**, *447*, 549.
(11) Voevodin, N. N.; Grebasch, N. T.; Soto, W. S.; Arnold, F. E.; Donley, M. S. *Surf. Coat. Technol.* **2001**, *140*, 24.
(12) Sheffer, M.; Groysman, A.; Starosvetsky, D.; Savchenko, N.; Mandler, D. *Corros. Sci.* **2004**, *46*, 2975.
(13) Garcia-Heras, M.; Jimenez-Morales, A.; Casal, B.; Galvan, J. C.; Radzki, S.; Villegas, M. A. *J. Alloys Compd.* **2004**, *380*, 219.
(14) Pepe, A.; Aparicio, M.; Cere, S.; Duran, A. *J. Non-Cryst. Solids* **2004**, *348*, 162.
(15) Osborne, J. H.; Blohowiak, K. Y.; Taylor, S. R.; Hunter, C.; Bierwagen, G.; Carlson, B.; Bernard, D.; Donley, M. S. *Prog. Org. Coat.* **2001**, *41*, 217.
(16) Palanivel, V.; Huang, Y.; van Ooij, W. J. *Prog. Org. Coat.* **2005**, *53*, 153.
(17) van Ooij, W. J.; Zhu, D.; Stacy, M.; Seth, A.; Mugada, T.; Gandhi, J.; Puomi, P. *Tsinghua Sci. Technol.* **2005**, *10*, 639.
(18) Vreugdenhil, A. J.; Woods, M. E. *Prog. Org. Coat.* **2005**, *53*, 119.
(19) Zheludkevich, M. L.; Serra, R.; Montemor, M. F.; Yasakau, K. A.; Miranda Salvado, I. M.; Ferreira, M. G. S. *Electrochim. Acta* **2005**, *51*, 208.
(20) Zheludkevich, M. L.; Serra, R.; Montemor, M. F.; Ferreira, M. G. S. *Electrochem. Commun.* **2005**, *8*, 836.
(21) Dry, C. M.; Corsaw, M. J. T. *Cem. Concr. Res.* **1998**, *28*, 1133.
(22) Decher, G.; Hong, J. D.; Schmitt, J. *Thin Solid Films* **1992**, *210/211*, 831.
(23) Clark, S. L.; Handy, E. S.; Rubner, M. F.; Hammond, P. T. *Adv. Mater.* **1999**, *11*, 1031.
(24) Yamauchi, F.; Kato, K.; Iwata, H. *Langmuir* **2005**, *21*, 8360.
(25) Coche-Guerente, L.; Desbrieres, J.; Fatisson, J.; Labbe, P.; Rodriguez, M. C. *Electrochim. Acta* **2005**, *50*, 2865.
(26) Ai, H.; Meng, H. D.; Ichinose, I.; Jones, S. A.; Mills, D. K.; Lvov, Y. M.; Qiao, X. X. *J. Neurosci. Methods* **2003**, *128*, 1−8.
(27) Farhat, T. R.; Hammond, P. T. *Adv. Funct. Mater.* **2005**, *15*, 945.
(28) Yu, A. M.; Liang, Z. J.; Caruso, F. *Chem. Mater.* **2005**, *17*, 171.
(29) Wang, L. Y.; Schönhoff, M.; Möhwald, H. *J. Phys. Chem. B* **2002**, *106*, 9135.
(30) Joly, S.; Kane, R.; Rubner, M. F. *Langmuir* **2000**, *16*, 1354.
(31) Shchukin, D. G.; Sukhorukov, G. B.; Möhwald, H. *Chem. Mater.* **2003**, *15*, 3947.
(32) Shchukin, D. G.; Sukhorukov, G. B. *Adv. Mater.* **2004**, *16*, 671.
(33) Skirtach, A. G.; Dejugnat, C.; Braun, D.; Susha, A. S.; Rogach, A. L.; Parak, W. J.; Möhwald, H.; Sukhorukov, G. B. *Nano Lett.* **2005**, *5*, 1371.
(34) Lu, Z. H.; Prouty, M. D.; Guo, Z. H.; Golub, V. O.; Kumar, C. S. S. R.; Lvov, Y. M. *Langmuir* **2005**, *21*, 2042.
(35) Angelatos, A. S.; Radt, B.; Caruso, F. *J. Phys. Chem. B* **2005**, *109*, 3071.
(36) Yasakau, K. A.; Zheludkevich, M. L.; Lamaka, S. V.; Ferreira, M. G. S. *J. Phys. Chem. B* **2006**, *110*, 5515.

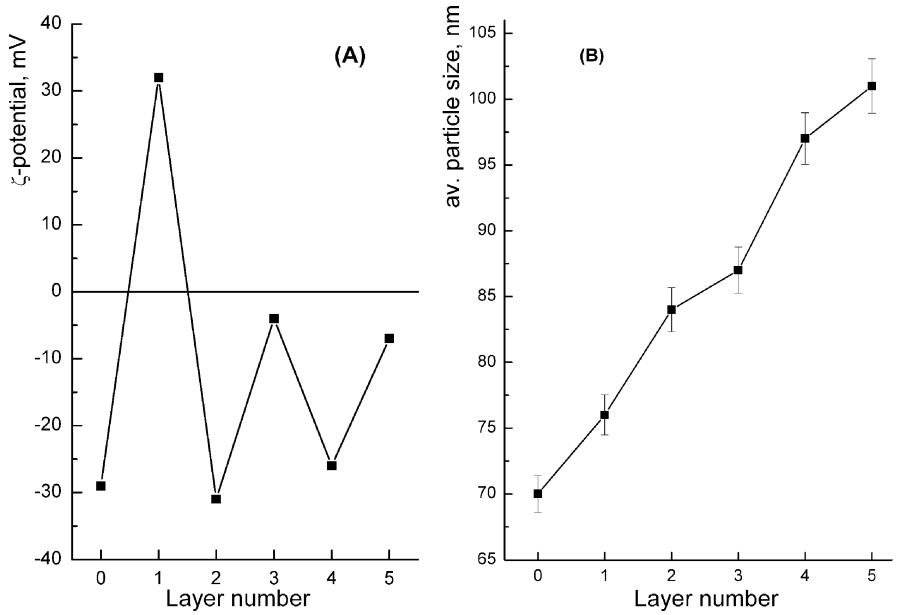

Figure 1. (a) Electrophoretic mobility measurements of nanocontainers: layer numbers of 0, initial SiO_2 particles; 1, SiO_2/PEI; 2, SiO_2/PEI/PSS; 3, SiO_2/PEI/PSS/benzotriazole; 4, SiO_2/PEI/PSS/benzotriazole/PSS; and 5, SiO_2/PEI/PSS/benzotriazole/PSS/benzotriazole. (b) Diameter of the nanocontainers vs LbL assembly step.

In the present work we demonstrate the possibility to employ 70 nm SiO_2 particles coated with poly(ethylene imine)/poly(styrene sulfonate) (PEI/PSS) layers as perspective nanocontainers embedded in hybrid epoxy-functionalized ZrO_2/SiO_2 sol−gel coatings. The inhibitor (benzotriazole) is entrapped within polyelectrolyte multilayers in the assembly step. The resulting hybrid film has a pronounced protective efficiency and self-healing effect. The release of the inhibitor is initiated by pH changes in defective areas during corrosion of AA2024 aluminum alloy employed as a model substrate.

2. Experimental Section

2.1. Materials. A more detailed composition of the aluminum alloy AA2024 is described in ref 9. An alkaline cleaner TURCO 4215 (from TURCO S.A., Spain) that contains sodium tetraborate and sodium tripolyphosphate mixed with a combination of surfactants was used to clean the aluminum alloy before deposition of the anticorrosion coating. Sodium PSS (molecular weight ∼ 70 000), PEI (molecular weight ∼ 2000), benzotriazole, HCl, NaCl, zirconium *n*-propoxide (TPOZ), 3-glycidoxypropyltrimethoxysilane (GPTMS), propanol, ethylacetoacetate, and HNO_3 were purchased from Sigma-Aldrich. LUDOX HS colloidal silica (40% suspension in water; DuPont, France) was used as a source of silica nanoparticles. The water was purified in a three-stage Millipore Milli-Q Plus 185 purification system and had a resistivity higher than 18 MΩ·m.

2.2. Preparation of Nanocontainers. To produce an inhibitor-impregnated polyelectrolyte shell, we followed the LbL deposition procedure involving both large polyelectrolyte molecules and small benzotriazole ones. The initial SiO_2 nanoparticles are negatively charged, and the deposition of the positive PEI (Figure 1) was performed on the first stage mixing 20 mL of SiO_2 (15 wt %) colloidal solution with 3 mL of 2 mg/mL PEI solution for 15 min. Then, the SiO_2/PEI sample was washed three times by centrifugation (Sigma 3K30) in distilled water. This washing procedure was performed after each deposition step. Deposition of the negative PSS layer was carried out from 2 mg/mL PSS solution in 0.5 M NaCl. Deposition of the third inhibitor layer (third) was accomplished in acidic media (pH = 3) from a 10 mg/mL solution of benzotriazole. The last two deposition steps (PSS and benzotriazole) were repeated once to ensure the highest inhibitor loading in the final LbL structure. The resulting nanocontainers have a SiO_2/PEI/PSS/benzotriazole/PSS/benzotriazole layer structure. The benzotriazole content in the nanocontainers is equal to 95 mg/1 g of the initial SiO_2 particles.

2.3. Synthesis and Deposition of Sol−Gel Films. In order to provide a comparative study of the effect of the benzotriazole corrosion inhibitor on the corrosion protection performance of the hybrid sol−gel films, the following composite films were synthesized: (i) an undoped hybrid SiO_x/ZrO_x based film; (ii) two sol−gel films doped with benzotriazole by direct impregnation of the inhibitor into the SiO_x/ZrO_x based film (two different concentrations of the benzotriazole, 0.13 wt % and 0.63 wt %, were taken for comparison); and (iii) two SiO_x/ZrO_x based films doped with different quantities of benzotriazole-impregnated nanocontainers.

The hybrid film was obtained by a controllable sol−gel route in *n*-propanol. Two different sols were combined together, forming a final sol, which was applied on the aluminum alloy. The first sol was prepared by hydrolyzing TPOZ (70 wt % TPOZ precursor in *n*-propanol) mixed with ethylacetoacetate (1:1 volume ratio) by addition of acidified water (pH < 1). At first the mixture of TPOZ and ethylacetoacetate was stirred under ultrasonic agitation at room temperature for 20 min to achieve complexation of the precursor. Then, acidified water in a 1:3 molar ratio (Zr/H_2O) was added to the mixture drop by drop, and the mixture was agitated for 1 h. The second organosiloxane sol was obtained by hydrolyzing GPTMS in 2-propanol by addition of acidified water in a 1:3:2 (GPTMS/2-propanol/water) molar ratio. In the final step, the zirconia-based sol was added drop by drop to the second organosiloxane sol in a 1:2 volume ratio. The resulting sol−gel system was ultrasonically agitated for 60 min and aged for 1 h at room temperature before deposition on the aluminum alloy. Water-based solutions of benzotriazole or the colloid solution of the nanocontainers with adjusted pH value were used instead of acidified water to obtain the first zirconia-based sol. Different concentrations of benzotriazole or nanocontainers were used to obtain different amounts of inhibitor loading. The concentration of the nanocontainers in the final sol−gel system was two times lower in the

case of the low loading when compared to that for the high-impregnated sample.

The AA2024 sheets were pre-cleaned in 60 g/L of TURCO 4215 solution for 15 min at 60 °C followed by a 15 min immersion in 20% nitric acid. The sol−gel films were deposited on the surface of AA2024 by the dip-coating procedure, immersing the substrate in the final sol−gel mixture for 100 s followed by its controlled withdrawal with a speed of 18 cm/min. Coated AA2024 was cured at 130 °C in air for 1 h.

2.4. Experimental Methods. The structure of the sol−gel coatings before and after immersion was studied by scanning electron microscopy (SEM; Hitachi S-4100 system with electron beam energy of 25 keV). The size and electrophoretic mobility measurements of the nanocontainers were performed using a Malvern Zetasizer 4. The topography of the hybrid films containing nanocontainers was revealed by an atomic force microscope (Nanoscope Digital Instruments) equipped with a NanoScope III controller in tapping mode. The viscosity of the sols was measured by a rotational CSL Rheomiter at the shear rate 600 s^{-1}.

Electrochemical impedance spectroscopy (Gamry FAS2 Femtostat with a PCI4 Controller) was employed to assess the corrosion performance of the developed hybrid sol−gel films on AA2024-T3 immersed in 0.005 and 0.5 M NaCl solutions. A conventional three-electrode cell with a saturated calomel reference electrode in a Faraday cage was used. A platinum foil was employed as the counter electrode, and the samples under study (exposed surface area of 3.4 cm^2) were used as a working electrode. The impedance measurements were performed at the open circuit potential with applied 10 mV sinusoidal perturbations in the frequency range of 10^{-2}−10^5 Hz with 10 steps per decade. The impedance plots were fitted with a compatible equivalent circuit that mimics the aluminum alloy during the corrosion process.

The scanning vibrating electrode technique (SVET) measurements were performed in 0.05 M NaCl using an apparatus manufactured by Applicable Electronics, Inc. (U.S.A.), controlled by the ASET software developed by ScienceWares, Inc. (U.S.A.), and employed microelectrodes of MicroProbes, Inc. (U.S.A.). SVET measures the potential differences in solution due to the ionic fluxes that arise from the electrochemical reactions occurring in the corroding metal surface. The measured potential differences, ΔV, can be related to the ionic currents that originate them, I, by a proper calibration. The microelectrode had a spherical black platinum tip of 10 μm in diameter and vibrated in two directions (normal and parallel to the surface) with an amplitude of 20 μm and with the probe vibrating average distance of 200 μm above the sample. In each point the system waited 0.2 s before measurement, and the sampling time was 0.4 s. All data were recorded by ASET in the computer. Experimental results were presented in the form of two-dimensional maps of ionic currents. The maps were generated by the QuikGrid program (freeware, www.perspectiveedge.com) using data from the electric field normal to the surface. Positive (red) values correspond to anodic activity, and negative values (blue) correspond to cathodic activity.

3. Results and Discussion

Nanocontainers. Electrophoretic measurements indicate the charging of the nanoparticles coated with the adsorbed polyelectrolyte or inhibitor layer upon each added layer. Figure 1a represents a drastic increase of the surface charge after deposition of the first PEI layer (65 mV) followed by a similar (68 mV) decrease after PSS adsorption in the next stage. Benzotriazole deposition leads to a less pronounced increase of the ζ-potential without complete recharging of the surface. This is caused by the different molecular weight, charge, and size of the layer components. Large multicharged chains of PEI or PSS have stronger electrostatic forces and can be adsorbed in quantities sufficient to completely recharge the surface while small molecules of monocharged benzotriazole only compensate the excess of negative charge resulting in a PSS/benzotriazole complex insoluble in slightly acidic and neutral water solutions. The average diameter of the nanocontainers obtained from light scattering measurements increases with the layer number (Figure 1b), which clearly indicates the LbL assembly of polyelectrolytes and inhibitor molecules. For the first PEI and PSS monolayers the size increment is about 8 nm per layer. The benzotriazole layers increase the size of nanocontainers by a smaller (∼4 nm) step confirming the electrophoretic mobility data on a lower amount of deposited benzotriazole as compared to the polyelectrolytes. The optimal number of the PSS/benzotriazole bilayers deposited onto silica nanoparticles is two. One bilayer is not sufficient for the self-healing effect of the final protective coating while three or more bilayers drastically increase the aggregation of nanocontainers during assembly and coating deposition, which affects the integrity of the protective coating and nanocontainers distribution in the coating matrix adversely.

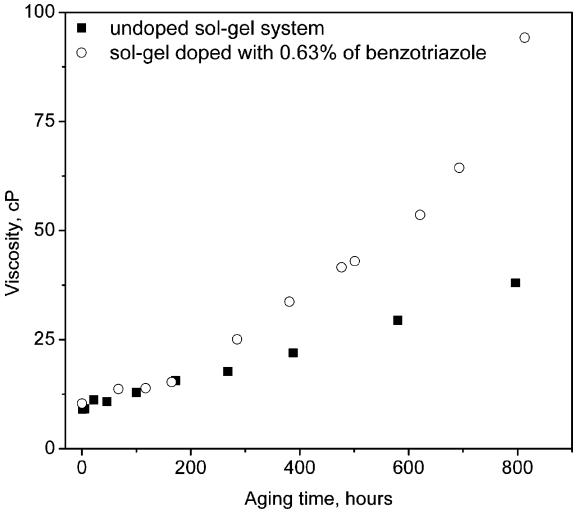

Figure 2. Viscosity evolution for hybrid sols during aging.

Characterization of the Nanocomposite Coatings. The stability of the sol−gel solution before deposition of the thin films is an issue of prime importance for reproducible film characteristics. Substrate dipping during the transition period of the SiO_x/ZrO_x sol near the gelation point can cause formation of hybrid films with quite different properties such as thickness, density changes after shrinkage, tendency toward crack formation, and so forth. Therefore, the evolution of the viscosity of the obtained alcosols was monitored. Figure 2 compares viscosity of the SiO_x/ZrO_x sol with and without benzotriazole. Both sols have a similar viscosity values immediately after synthesis and exhibit a small linear increase within the first 200 h of aging, showing that the systems are far from the gelation point. The dipping procedure was performed in freshly prepared sol immediately after its synthesis. The addition of benzotriazole does not significantly influence the sol viscosity at this period. The gelation of the hybrid undoped alcosol does not occur even

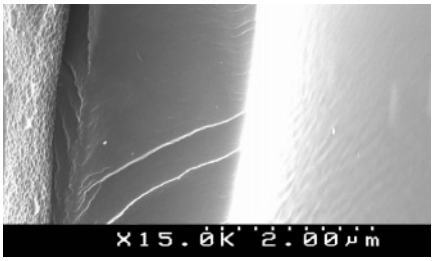

Figure 3. Cross-sectional electron micrograph of the undoped sol−gel film on the AA2024 substrate.

after 800 h of aging, whereas for a benzotriazole containing sol the gelation starts approximately after 400 h. The thickness of the obtained hybrid films was estimated with cross-sectional SEM analysis as shown in Figure 3. The average thickness of about 1.8−2.0 μm was found for different films regardless of the composition.

The atomic force microscopy (AFM) scan in Figure 4a taken before immersion of the coated aluminum in NaCl solution reveals the topography of the hybrid film doped with nanocontainers. Only a few particle-like features with a diameter of about 100 nm can be seen on the surface. The SEM observation (Figure 4c) confirms the presence of such particles in the film. This proves the occlusion of the majority of the nanocontainers inside the film volume confirming good affinity of SiO_2-based nanocontainers to ZrO_x/SiO_x film. The same sample was also examined by AFM after 2 weeks of immersion in NaCl solution. Figure 4b demonstrates the topography of the composite film after treatment in aggressive media. A high concentration of nanoparticles is present on the surface. The image (Figure 4d) acquired at higher magnification shows that these particles are 70−100 nm in diameter, which is close to the diameter of the nanocontainers before loading in the coating. The increased number of nanocontainers visible in the AFM image upon NaCl treatment can be caused by dissolution of the top layer of the sol−gel film opening the embedded nanocontainers. These nanocontainers are uniformly distributed in the sol−gel film (Figure 4b,d) showing low degree of aggregation. One can conclude the proposed protocol results in formation of reproducible, uniform, and dense ZrO_x/SiO_x films with evenly distributed SiO_2-based nanocontainers.

Corrosion Performance of the Nanocomposite Coatings. The main function of the developed coatings is active and passive corrosion protection. Figure 5 presents optical photos of the two aluminum samples: the first one was coated by a sol−gel film with benzotriazole directly introduced into the ZrO_x/SiO_x matrix, and second one was coated by the nanocomposite film impregnated with nanocontainers. The first sample shows many pit-like defects formed on the surface exhibiting very weak corrosion protection even in diluted 0.005 M NaCl solution. The second sample that contains nanocontainers does not exhibit any visible signs of corrosion attack even after 14 days in 100 times more concentrated solution (0.5% NaCl). This pronounced difference shows the advantages of the "nanocontainer" approach over the direct introduction of inhibitor in the sol−gel coating.

Electrochemical impedance spectroscopy was employed to quantify the difference in the corrosion protection obtained by the different composite coatings under study. The dependence of the complex impedance of the coated aluminum on the frequency applied allows the separation of

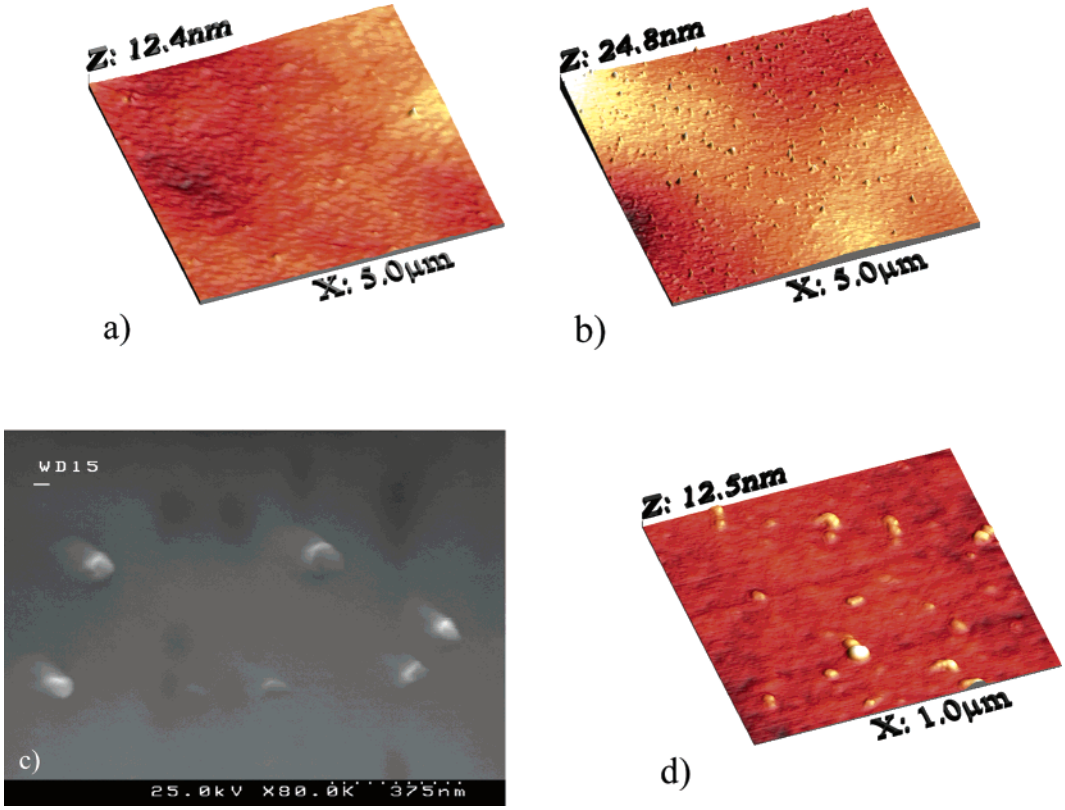

Figure 4. Micrograph and topography images of the hybrid films doped with higher amounts of nanocontainers obtained by SEM (c) and AFM (a, b, d,) before (a, c) and after 14 days (b, d) of immersion in NaCl.

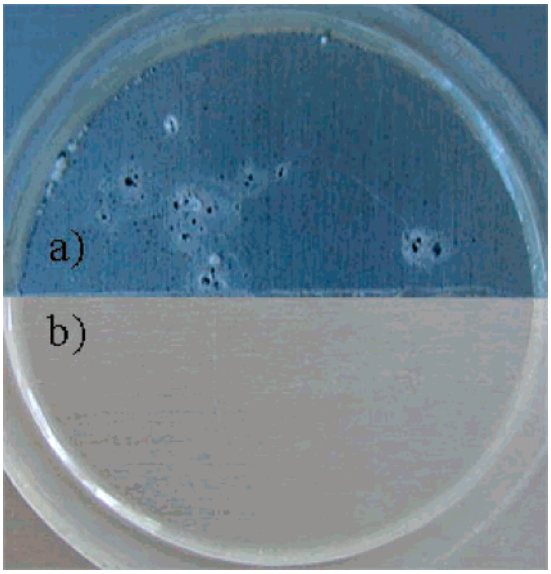

Figure 5. 2024 aluminum alloy coated with sol−gel film directly doped with benzotriazole (a) and with sol−gel film doped with nanocontainers (b) after 14 days of immersion in 0.005 M NaCl (a) and 0.5 M NaCl (b).

the response of the different components of the system such as capacitance and resistance of the protective layers, polarization resistance, and double layer capacitance. The evolution of these parameters during the corrosion process can distinguish passive and active corrosion protection of the different coatings.

Figure 6 depicts a typical impedance spectrum of the AA2024 alloy coated with a composite sol−gel film. Three time constants are present in the spectrum after 2 weeks of immersion in 0.5 M NaCl. The high-frequency time-dependent component at about 10^5 Hz is related to the capacitance of the composite sol−gel layer.[19] This interpretation is also supported by the fact that the increase of the withdrawal speed during coating deposition leads to a higher thickness of the film and, consequently, to a decrease of the capacitance at high frequencies (not shown), the rest of the spectrum remaining unchanged. According to the physical model of similar protective coatings,[19] the equivalent circuit was constructed as shown in the inset in Figure 6. Here, constant phase elements were used instead of capacitances in order to take into account the dispersive character of the time constants originating from the nonuniformity of the layers. Then the true capacitance was calculated using the equation proposed elsewhere.[37] The resistive plateau at 10^2−10^3 Hz represents the pore resistance of this sol−gel film. The time constant at about 1 Hz originates from the capacitance of the intermediate oxide layer between the metal surface and the sol−gel film. In several experiments aluminum substrates were heat-treated at 250 °C prior to the coating deposition in order to increase the thickness of the aluminum oxide film on the substrate. However, such a treatment leads only to increase of the capacitance of the medium time constant without any changes in the remaining spectrum (not shown). This fact confirms once again that the time dependent component at about 1 Hz appears due to the capacitance of the intermediate oxide layer. Other relaxation processes observable at the low frequencies of the spectrum originate from the corrosion processes starting in the defects induced in the oxide layer.[19]

Figure 7 depicts the impedance spectra of all samples after 190 h of immersion in 0.005 M NaCl. The undoped hybrid film and the coatings doped with different concentrations of nanocontainers show very similar behavior at frequencies higher than 0.1 Hz revealing the same barrier properties. The capacitance of the oxide layer is also the same for those samples. A significant difference appears only at low frequencies, which is related to the open defects in the Al_2O_3 intermediate layer and, consequently, corrosion activity as well. The sample with highest concentration of nanocontainers in the matrix shows almost pure capacitative behavior at low frequencies demonstrating excellent protective properties even after long immersion time. This confirms the absence of active defects. The sample with lower concentration of nanocontainers also demonstrates a good corrosion protection performance. However, the resistive part appears at low frequencies demonstrating the formation of active defects. The AA2024 coated with undoped ZrO_x/SiO_x film

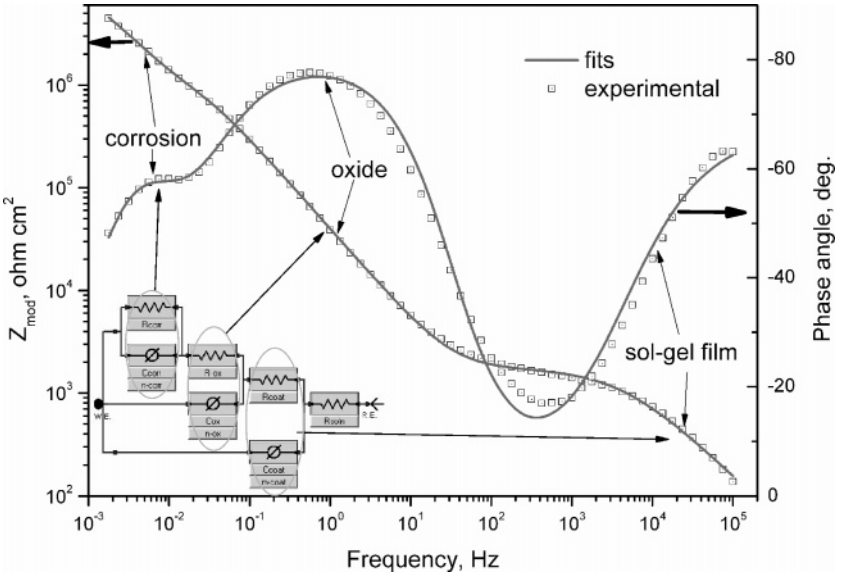

Figure 6. Impedance spectrum of AA2024 coated with undoped sol−gel film after 14 days of immersion in 0.5 M NaCl: The inset reveals the equivalent circuit used for spectrum fitting.

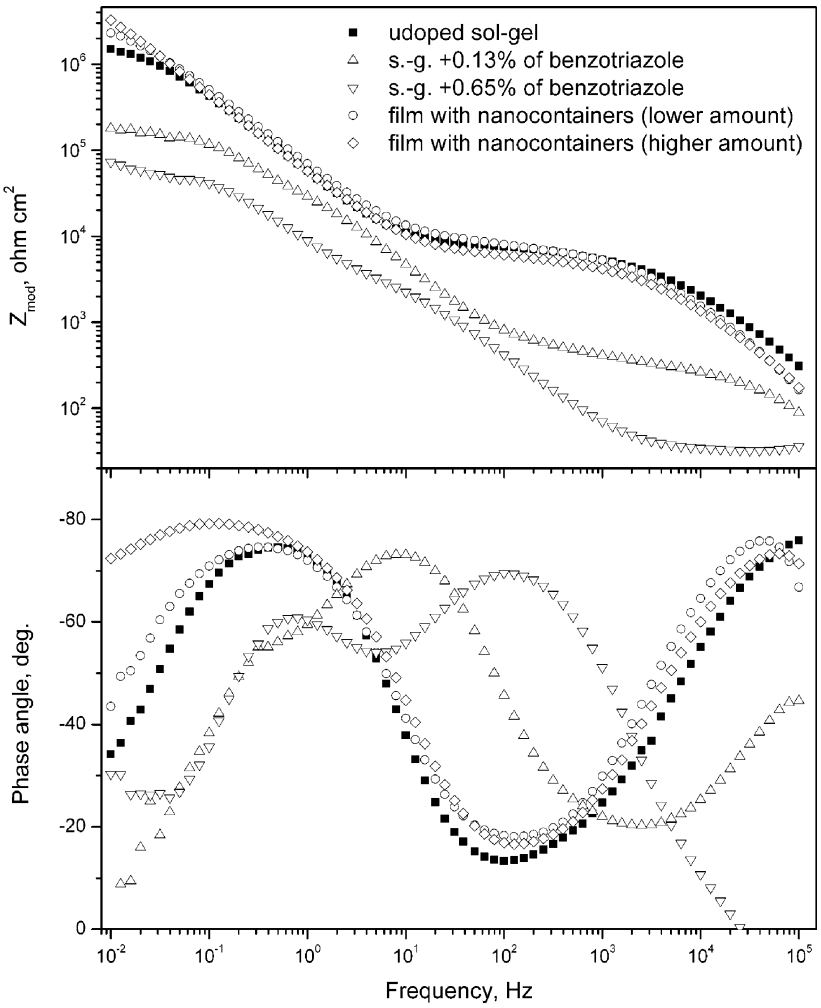

Figure 7. Impedance spectra of different sol−gel films after 190 h of immersion in 0.005 M NaCl.

shows lower corrosion resistance than in both previous cases. The results clearly illustrate the positive effect of the nanocontainers impregnated with benzotriazole on the corrosion protection performance of the ZrO_x/SiO_x sol−gel films. The effect increases with the increase of the loading degree of the nanocontainers.

Two other samples prepared by direct impregnation of the benzotriazole molecules into the sol−gel matrix show very low corrosion protection performance (Figure 7). The sol−gel film with 0.13% of inhibitor has 1 order of magnitude lower resistance demonstrating defective character of the film. The high-frequency time constant completely disappears from the spectrum of the film doped with 0.63% of benzotriazole. Apparently, the inhibitor has a detrimental effect on the sol−gel process, which is prevented when it is fixed in the nanocontainer shell. This occurs since the resistance of the sol−gel film is comparable with the resistance of the electrolyte. The third time constant originated from the active corrosion processes is well defined showing poor protective behavior of the ZrO_x/SiO_x films directly doped with benzotriazole during the sol−gel synthesis.

The low concentration of NaCl was used in this study in order to decrease the rate of the corrosion processes in the case of the samples with weak corrosion protection performance. The decrease of the salt concentration decreases the rate of the corrosion processes and allows the estimation of its kinetics. Moreover, additional long-term experiments were performed for the undoped film and the coating with the maximal content of nanocontainers in the 0.5 M NaCl, which is a very strongly corrosive electrolyte. Figure 8 demonstrates the impedance spectra of these samples after 270 h of immersion. Both coatings still provide effective corrosion protection in spite of the high electrolyte concentration. However, the film with nanocontainers performs better than the undoped hybrid coating.

The evolution of both the sol−gel film resistance and the oxide layer resistance was analyzed for all the samples under study in order to estimate the kinetics of the system degradation during the corrosion process (Figure 9). The resistance of the dielectric sol−gel film is determined by the resistance of the electrolyte in the pores, which form conductive pathways. Hence, the monitoring of the film resistance during immersion can give quantitative information on the barrier properties and stability of the film. The time-dependent evolution of the resistance of the composite sol−gel films is depicted in Figure 9a. At the beginning the sol−gel films have similar resistances of about 10^5 Ω·cm^2. However, a fast decrease occurs during the first hours of immersion. This drop is caused by the filling of the micro-

(37) Hsu, C. S.; Mansfeld, F. *Corrosion* **2001**, *57*, 747.

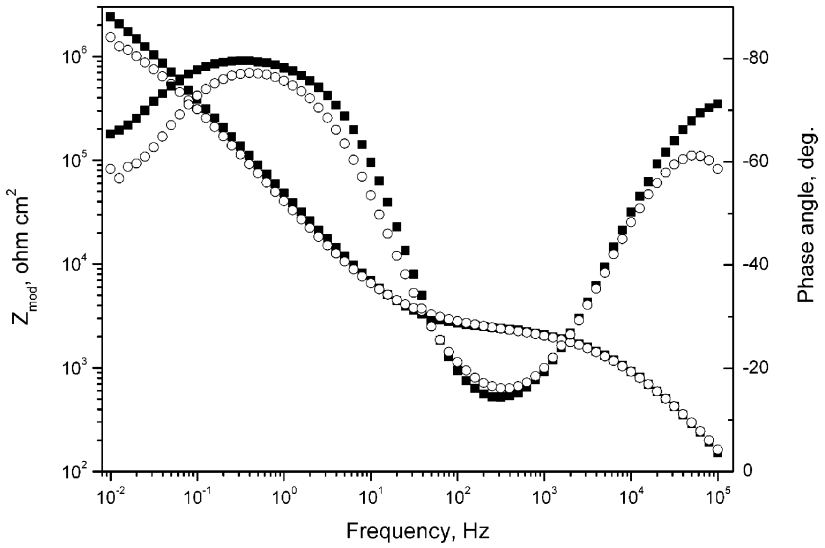

Figure 8. Impedance spectra of the undoped sol−gel film (○) and coating with higher concentration of nanocontainers (■) after 270 h of immersion in 0.5 M NaCl solution.

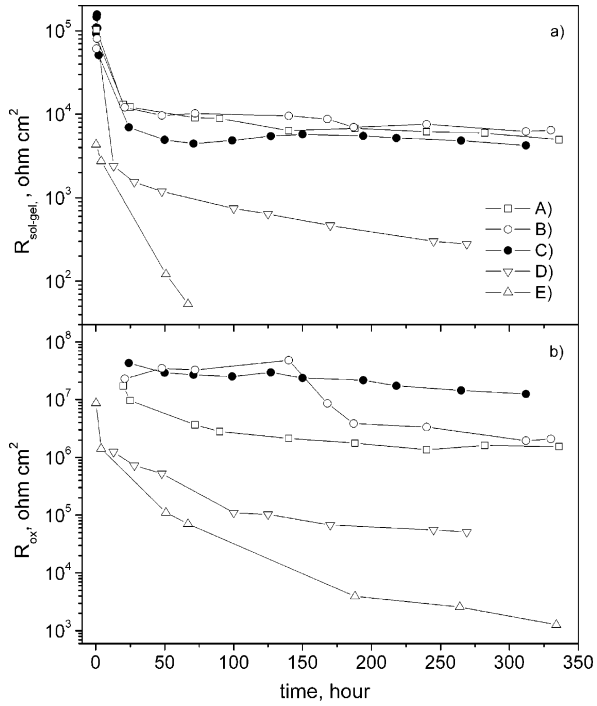

Figure 9. Evolution of the sol−gel film resistance (a) and resistance of the intermediate oxide layer (b) in 0.005 M NaCl electrolyte for AA2024 coated with the following hybrid films: (A) undoped sol−gel film; (B) coating with lower concentration of nanocontainers; (C) coating with higher concentration of nanocontainers; (D) film with sol−gel matrix directly doped with 0.13% of benzotriazole; and (E) coating with the sol−gel matrix directly doped by 0.63% of benzotriazole.

and nanopores of the film with electrolyte. The undoped sol−gel film and the coatings doped with different amounts of nanocontainers demonstrate very close values of pore resistance confirming that the introduction of the nanocontainers does not influence the porosity and density of the composite matrix. The stable behavior of the pore resistance during the next 300 h confirms the high hydrolytic stability of the sol−gel film. On the other hand, the films with direct addition of benzotriazole show sufficiently higher porosity. The difference in the coating resistances is 1 order of magnitude for a 0.13% concentration of benzotriazole. The film resistance drops with the immersion time proving fast degradation of the film. Addition of higher concentration of benzotriazole (0.63%) leads to the formation of noncompact films with very poor weathering stability.

The role of the nanocontainers is not only to diminish the negative effect in the inhibitor on the polymer film but also to provide delivery of inhibitor on demand and to ensure the active corrosion protection when defects are formed in the coating. The resistance of the oxide layer can be a parameter that permits monitoring of the corrosion protection because it is proportional to the metal surface area in contact with the electrolyte. Figure 9b demonstrates the evolution of the oxide layer resistance for all the samples during immersion in the chloride-based electrolytes. The highest values of the oxide resistance were found for samples doped with nanocontainers. This superior corrosion protection performance evidently originates from the inhibiting effect of the benzotriazole released from the nanocontainers. However, the resistance of sample impregnated with lower content of nanocontainers decreases by 1 order of magnitude after about 150 h due to the release and consumption of the inhibitor while the coating with higher loading has very stable long-term behavior. The oxide layer resistance in the more concentrated NaCl solution for the sample with the maximal concentration of nanocontainers (not shown) is about 2 times lower but still is 10 times higher than that of the undoped ZrO_x/SiO_x sample in diluted 0.005 M NaCl. This difference remains even after 300 h of immersion demonstrating effective long-term corrosion protection of nanocontainer-impregnated sample. Also, both samples prepared by direct introduction of benzotriazole into the sol−gel film show poor corrosion protection performance. The low values of the oxide layer resistance suggest absence of any inhibiting effect. This fact can be explained by interaction of the benzotriazole with components of the coating during the sol−gel synthesis, which leads to deactivation of the inhibitor molecules.

The higher corrosion protection of the films doped with benzotriazole-impregnated nanocontainers can be originated from the inhibiting action of the benzotriazole molecules

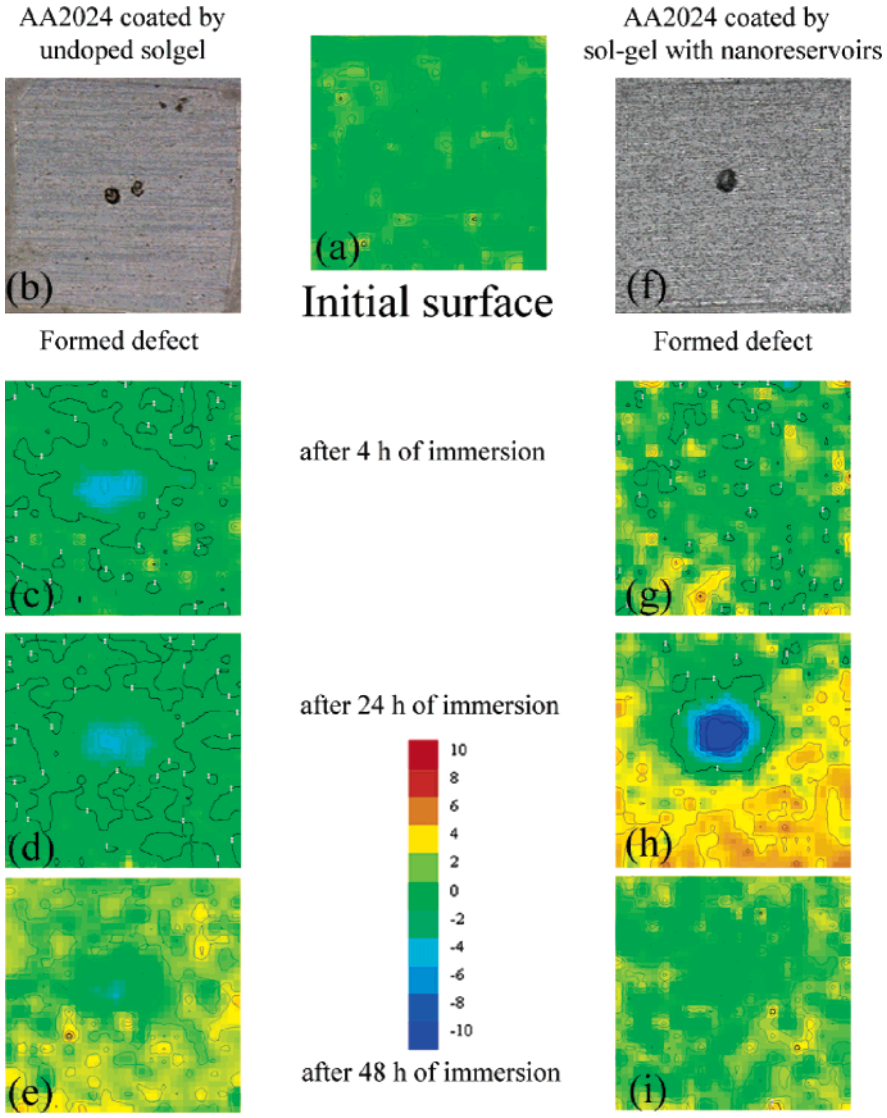

Figure 10. SVET maps of the ionic currents measured above the surface of the AA2024 coated with undoped sol−gel pretreatment (a, c, d, e) and with pretreatments impregnated by nanocontainers (g−i). The maps were obtained before defect formation (a) and for 4 h (c, g), 24 h (d, h) and 48 h (e, i) after defect formation. Scale units: μA cm^{-2}. Scanned area: 2 mm × 2 mm.

released from the nanocontainers in a controlled way. Benzotriazole was recently found as an effective corrosion inhibitor for AA2024 alloy in chloride solutions.[38] The benzotriazole is absorbed on the alloy surface preventing chemisorption of chloride anions. The benzotriazole molecules also decrease the rate of the cathodic oxygen reduction on copper-rich intermetallic particles.

Self-Healing Ability of the Nanocomposite Coatings. The electrochemical impedance spectroscopy measurements demonstrate the superior corrosion protection of the sol−gel films doped with benzotriazole-impregnated nanocontainers. However, the thin ZrO_x/SiO_x layer is used as a pretreatment and not as a full anticorrosion system. This pretreatment has three main functions: (i) to improve adhesion between the paints and the metal substrate; (ii) to provide an additional barrier to the corrosive species; and (iii) to perform active corrosion protection originated from self-healing of the defects induced in the top layer. The first function is achieved due to the formation of chemical Si−O−Al bonds on the metal/pretreatment interface. The barrier properties of the novel developed composite films were discussed above. The self-healing ability is the most important attribute of the effective pretreatment. Therefore, the self-healing efficiency of the ZrO_x/SiO_x films impregnated with inhibitor-impregnated nanocontainers was investigated by the SVET. The SVET method allows measuring the local fluxes of cations and anions along the surface. Generally, the corrosion processes generate ion flow on the cathodic and anodic zones of AA2024 as shown below.

Cathodic reactions generate hydroxyls

$$2H_2O + 2e^- \rightarrow 2OH^- + H_2\uparrow$$

$$O_2 + 2H_2O + 4e^- \rightarrow 4OH^-$$

while anodic processes lead to formation of metal cations

$$Al \rightarrow Al^{3+} + 3e^-$$

$$Mg \rightarrow Mg^{2+} + 2e^-$$

(38) Zheludkevich, M. L.; Yasakau, K. A.; Poznyak, S. K.; Ferreira, M. G. S. *Corros. Sci.* **2005**, *47*, 3011.

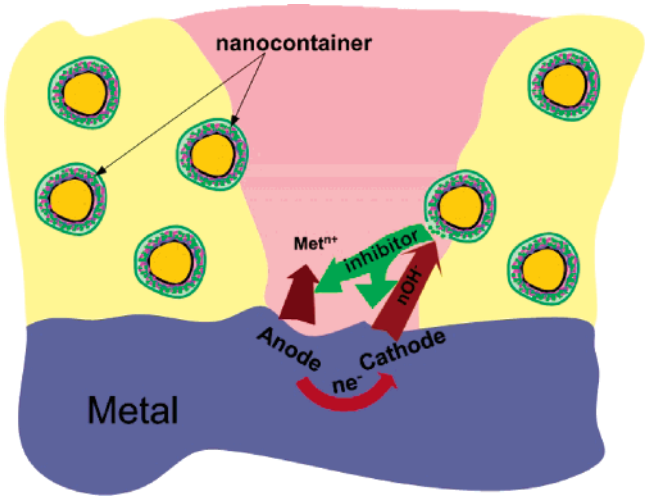

Figure 11. Scheme of the controllable release of the inhibitor from the nanocontainers and the "smart self-healing" process.

The local cathodic and anodic corrosion zones can be observed on the coated metal surface monitoring the local ionic flow densities. Figure 10 demonstrates the local current maps over the AA2024 alloy surface covered with both the undoped ZrO_x/SiO_x film and the ZrO_x/SiO_x film impregnated with the maximal amount of nanocontainers. A typical current map along the intact sol−gel film is depicted in Figure 10a illustrating the absence of local corrosion processes for both coatings. Artificial defects (200 μm in diameter) were formed on the surface of both coatings after 24 h of immersion in 0.05 M NaCl as shown in Figure 10b,f. Well-defined cathodic activity appears in the place of the induced defect on the alloy coated with the undoped hybrid film (Figure 10c). This activity becomes even more intense with the immersion time (Figure 10d,e). Sufficiently different behavior was revealed after defect formation on the substrate coated with the ZrO_x/SiO_x film doped with nanocontainers. No corrosion activity appears in this case after 4 h following the defect formation (Figure 10g). Only after about 24 h the well-defined cathodic activity appears in the zone of the induced defect (Figure 10h). The rest of the surface generates a cationic flow. However, the defect becomes passivated again 2 h later and remains healed even after 48 h (Figure 10i). One can see that local corrosion activity triggers the release of a portion of benzotriazole from the nanocontainers hindering the corrosion process in the defective area. Such a "smart" self-healing effect can be originated from the active feedback between the coating and the localized corrosion processes. The most probable mechanism is based on the local change of pH in the damaged area due to the corrosion processes. The permeability of the polyelectrolyte shells strongly depends on pH.[39] When the corrosion processes are started, the pH value is changed in the neighboring area, which opens the polyelectrolyte shell of the nanocontainers in a local area followed by release of benzotriazole. Then, the released inhibitor suppresses the corrosion activity as shown in Figure 10. As a result, the pH value becomes recovered closing the polyelectrolyte shell of the nanocontainers and terminating further release of the inhibitor. Thus the introduction of nanocontainers to the ZrO_x/SiO_x film leads to active corrosion protection originating from "smart" self-healing ability as schematically demonstrated in Figure 11. However, further investigations are necessary to prove the mechanism of self-healing provided by the nanocontainer-containing coatings.

4. Conclusions

A new method of corrosion inhibitor delivery on demand is proposed in this work conferring "intelligent" self-healing ability to the hybrid sol−gel protective films. Controllable delivery is achieved incorporating nanocontainers of benzotriazole inhibitor in the hybrid pretreatments. The nanocontainers were formed using silica nanoparticles LbL coated with polyelectrolyte molecules acting as nanocontainers of corrosion inhibitor.

The impregnation of the hybrid sol−gel films increases their long-term corrosion protection performance for metallic substrates. Moreover the introduction of the inhibitor in the form of nanocontainers instead of the direct addition to the sol−gel matrix prevents the interaction of the benzotriazole with components of the coating, which can negatively influence the barrier properties of the hybrid film and lead to the deactivation of the corrosion inhibitor. The sol−gel films doped with nanocontainers of corrosion inhibitors demonstrate very important self-healing ability conferring active corrosion protection to the hybrid pretreatments.

The use of the nanocontainer approach creates a new opportunity to substitute the carcinogenic chromates, allowing the development of a new generation of active corrosion protective systems possessing effective self-repairing capacity of the corrosion defects.

Acknowledgment. The authors acknowledge the financial of the work projects POCI/CTM/59234/2004 (FCT), EU FP6 "Nanocapsule" (Contract No. MIF1-CT-2004-002462), and CLG Grant CLG981299. The authors also thank P. Cecilio and M.F. Montemor (Instituto Superior Tecnico, Lisbon) for the SVET measurements.

CM062066K

(39) Antipov, A. A.; Sukhorukov, G. B. *Adv. Colloid Interface Sci.* **2004**, *111*, 49.